IET Communications

Research Article

IET Journals
The Institution of Engineering and Technology

Coverage analysis of downlink cellular orthogonal frequency-division multiple-access networks using moment generating functions

ISSN 1751-8628
Received on 27th January 2015
Revised on 10th July 2015
Accepted on 25th August 2015
doi: 10.1049/iet-com.2015.0102
www.ietdl.org

Jaeyong Son[1], Changkyu Seol[2], Kyungwhoon Cheun[1], Kyeongcheol Yang[1] ✉

[1]*Department of Electrical Engineering, Pohang University of Science and Technology, 77 Cheongam-Ro, Nam-Gu, Pohang, Gyeongbuk 790-784, Korea*
[2]*Samsung Electronics Co., Ltd., Suwon, Gyeonggi, Korea*
✉ *E-mail: kcyang@postech.ac.kr*

Abstract: In this study, the coverage of downlink cellular orthogonal frequency-division multiple-access networks transmitting one quadrature-amplitude modulation symbol per hop is analysed. The coverage probability is first defined by using an upper bound on the bit error rate (BER) of a bit-interleaved coded modulation system. Moreover then, the moment generating functions of the legacy Gaussian and Laplacian metrics (LMs) for soft-decision decoding of an employed error-correcting code are derived for computing the upper bound on the BER and the corresponding coverage probability of the networks. Numerical results demonstrate that due to the impulsive nature of the inter-cell interference for moderate-to-small cell loads, the networks using the LM for soft-decision decoding significantly outperform those employing the legacy Gaussian metric in terms of the achievable cell radius and the amount of the average transmit power reduction.

1 Introduction

Orthogonal frequency-division multiple-access (OFDMA) has been accepted in many cellular standards such as Institute of Electrical and Electronics Engineers (IEEE) 802.16e/m [1, 2] and third generation partnership project long term evolution (LTE) [3], since it possesses high spectral efficiency as well as it does not suffer from any *intracell* interference as long as the orthogonality among subcarriers is maintained. However, the coverage performance of downlink cellular OFDMA networks is mainly limited by the severe *intercell* interference (ICI) on the mobile stations (MSs) positioned at the cell edge [4]. The ICI may cause the reduction of the achievable cell radius or the increase of the average transmit power consumption.

Previous work [5–8] on the coverage analysis of downlink cellular OFDMA networks has dealt with the signal-to-interference-plus-noise ratio (SINR) as a major measure and has employed a Gaussian approximation of the sum of the ICI and the background noise, simply called the '*ICI-plus-noise*', as in code-division multiple-access networks [9]. However, the results in [10, 11] reveal that in downlink cellular OFDMA networks transmitting one quadrature-amplitude modulation (QAM) symbol per hop (simply, downlink subcarrier-hopping cellular OFDMA networks), the distribution of the ICI-plus-noise possesses a heavy tail and deviates significantly from the Gaussian distribution for moderate-to-small cell loads. This implies that the SINR may not be an appropriate measure for predicting the error rate or the coverage under such situations. It was also demonstrated in [10, 11] that decoders with non-Gaussian metrics based on the statistical characteristics of the ICI-plus-noise offer a significant performance gain over the decoder with the legacy Gaussian metric (GM) [12] for soft-decision decoding of an error-correcting code (ECC). For these reasons, it is challenging to quantify the coverage performance of downlink subcarrier-hopping cellular OFDMA networks employing a non-GM for soft-decision decoding.

In this paper, we analyse the coverage performance of downlink subcarrier-hopping cellular OFDMA networks employing the legacy Gaussian or Laplacian metrics (LMs) for soft-decision decoding of an ECC, based on the union bound on the bit error rate (BER) of a bit-interleaved coded modulation (BICM) system with quarternary phase-shift keying (QPSK) modulation or 16-ary QAM. Throughout this paper, the Gaussian (Laplacian, resp.) metric of a bit denotes its log-likelihood ratio (LLR) under the assumption that the real and imaginary parts of the ICI-plus-noise are approximated as independent and identically distributed (i.i.d.) Gaussian (Laplacian, resp.) random variables (RVs). The union bound on the BER of a BICM system employing legacy GM was computed in [13]. However, there are no known results on the BER of that employing non-GM. In downlink subcarrier-hopping cellular OFDMA networks, the LM as a simple non-GM is observed to exhibit much better performance than the GM for moderate-to-small cell loads. Moreover, it allows one to compute a bound on the BER of a BICM system. Therefore, it is employed as a non-GM for our coverage analysis in this paper. The moment generating functions (MGFs) of the GM and the LM for QPSK modulation or 16-ary QAM are derived and employed for computing an upper bound on the BER of a BICM system. On the basis of the bound, the coverage performance of downlink subcarrier-hopping cellular OFDMA networks is evaluated.

Numerical results demonstrate that the cell radius of the networks with QPSK modulation and 16-ary QAM increases by at least 40% and 180%, respectively, and the average base station (BS) transmit power can be reduced by at least 6 dB for all the considered cases, when the LM is employed instead of the GM. Our approach can be extended to the cases of 64-ary or 256-ary QAM, even though these cases are not included here due to the limit of space. Since the performance of the LM is far from the optimum decoding performance in downlink subcarrier-hopping cellular OFDMA networks, it is expected that the coverage performance may be further improved with a non-GM.

The remainder of this paper is organised as follows. Section 2 briefly describes the system model. The coverage probability based on the upper bound on the BER of a BICM system is defined in Section 3. In Section 4, the MGFs of the GM and the LM for QPSK modulation or 16-ary QAM are derived for computing the upper bound on the BER. Numerical results on the coverage performance of downlink cellular OFDMA networks with QPSK modulation or 16-ary QAM are presented in Section 5. Finally, concluding remarks are given in Section 6.

2 System model

Consider a synchronous, downlink cellular OFDMA network with N_B BSs. It is assumed that one QAM symbol per MS is transmitted in one of the available subcarriers in each OFDM symbol where the chosen subcarriers are taken randomly among the available subcarriers. Each BS sends K QAM symbols (hence, supporting K MSs) in K subcarriers in each OFDM symbol occupying a total of N ($\geq K$) subcarriers, where N is equal to the fast Fourier transform (FFT) size. Each OFDM symbol is prepended with a cyclic prefix of length G, measured in OFDM samples.

Let $c_{m,k}$ denote the M-ary QAM (M-QAM for short) symbol transmitted by the mth BS on the kth subcarrier with $\mathbb{E}(c_{m,k}) = 0$ and $\mathbb{E}(c^*_{m,k} c_{n,l}) = \delta_{m,n}\delta_{k,l}$ where $\mathbb{E}(\cdot)$ is the expectation operator, and $\delta_{m,n} = 1$ if $m = n$, and zero otherwise. Moreover, let $E_{\mathrm{s},m} \triangleq \gamma_m E_{\mathrm{T}}$ be the average received signal energy per subcarrier by the desired MS from the mth BS where E_{T} denotes the average transmitted signal energy per subcarrier at each BS, given by $E_{\mathrm{T}} \triangleq (A_{\mathrm{B}}/W\lambda)$ with A_{B} the average transmit power, W the signal bandwidth, and $\lambda \triangleq K/N$ the cell load. The factor, $\gamma_m \triangleq 10^{(\eta_m - \rho - 10\mu\log_{10} r_m)/10}$ represents the coefficient considering the path loss and the shadowing where η_m is a zero-mean Gaussian RV with σ_{S} the shadowing standard deviation, ρ is the path loss [in decibel (dB)] at 1 km, μ is the path loss exponent, and r_m is the Euclidean distance [in kilometre (km)] between the mth BS and the desired MS. Since the variations in the shadowing and the location of the MS are expected to be very slow, γ_m, $m = 1, \ldots, N_B$, are assumed to remain constant during the transmission of a codeword of the ECC employed in the underlying OFDMA network. This system model is identical to that described in [10], except that only QPSK modulation or 16-QAM is considered in this paper. The readers are referred to [10] for a more detailed description.

Assuming that the desired MS is perfectly synchronised with the selected BS possessing the maximum average signal strength, that is, $\max_{m=1,\ldots,N_B}\{\gamma_m\}$, the normalised FFT output at the kth subcarrier of a given OFDM symbol is given in [10] by

$$Y[k] = H_{\hat{m}}[k]c_{\hat{m},k} + Z[k] \tag{1}$$

for $k \in C_{\hat{m}}$, where $\hat{m}$ denotes the index of the selected BS, that is, $\hat{m} \triangleq \arg\max_{m=1,\ldots,N_B}\{\gamma_m\}$, C_m is the set of subcarrier indices occupied by the mth BS during the OFDM symbol duration, and

$$Z[k] \triangleq \sum_{m=1, m\neq\hat{m}}^{N_B} \sqrt{I_m} H_m[k] c_{m,k} p_{m,k} + \frac{W[k]}{\sqrt{E_{\mathrm{s},\hat{m}}}}$$

represents the combined effect of the ICI and the additive white Gaussian noise (AWGN), simply called the '*ICI-plus-noise*'. The factor $H_m[k]$ is the complex channel frequency response at the kth subcarrier between the mth BS and the desired MS, which is characterised by a circularly symmetric, zero-mean complex Gaussian RV with $\mathbb{E}(H^*_m[k]H_{m'}[k']) = \delta_{m,m'}\delta_{k,k'}$. The factor $W[k]$ represents the effect of the AWGN and is modelled as a zero-mean complex Gaussian noise process with $\mathbb{E}(W^*[k]W[l]) = N_0\delta_{k,l}$ where $N_0/2$ is the two-sided power spectral density of the AWGN, given by $N_0 \triangleq k_{\mathrm{B}}T(F-1)$ with k_{B} the Boltzmann constant, T the absolute temperature, and F the noise figure of the desired MS [14]. Moreover, $I_m \triangleq E_{\mathrm{s},m}/E_{\mathrm{s},\hat{m}} = \gamma_m/\gamma_{\hat{m}}$ represents the average power ratio of the mth BS to the selected BS, and $p_{m,k} = 1$ if $k \in C_m$, and zero otherwise.

The probability density function (PDF) of the ICI-plus-noise $Z[k]$, conditioned on $\boldsymbol{I} \triangleq [I_1, \ldots, I_{\hat{m}-1}, I_{\hat{m}+1}, \ldots, I_{N_B}]$ and λ, is derived in [10], but is complicated to exactly compute. Instead, the conditional PDF of the ICI-plus-noise assuming that all interfering cells employ a constant energy signal constellation is used in this paper, as in [10] where this approximation is justified by the fact that the uncoded symbol error rate based on (2) is shown to be very close to the simulation results even in the case of 16-QAM. That is, we have

$$f_{Z[k]}(z|\boldsymbol{I},\ \lambda) = \sum_{p_{1,k}=0}^{1} \cdots \sum_{p_{\hat{m}-1,k}=0}^{1} \sum_{p_{\hat{m}+1,k}=0}^{1} \cdots \sum_{p_{N_B,k}=0}^{1} \frac{\prod_{m=1,m\neq\hat{m}}^{N_B}((1-\lambda)(1-p_{m,k}) + \lambda p_{m,k})}{\pi \Upsilon_{P_k,I,\lambda}} \times \exp\left(-\frac{|z|^2}{\Upsilon_{P_k,I,\lambda}}\right) \tag{2}$$

where

$$\Upsilon_{P_k,I,\lambda} \triangleq \mathbb{E}\left(|Z[k]|^2 | \boldsymbol{P}_k,\ \boldsymbol{I},\ \lambda\right) = \sum_{m=1,m\neq\hat{m}}^{N_B} I_m p_{m,k} + \frac{N_0}{E_{\mathrm{s},\hat{m}}}$$

and $\boldsymbol{P}_k \triangleq [p_{1,k},\ \ldots,\ p_{\hat{m}-1,k},\ p_{\hat{m}+1,k},\ \ldots,\ p_{N_B,k}]$.

3 Coverage probability of the underlying OFDMA network

In this section, we will introduce a method to compute an upper bound on the BER of a convolutional code by using the MGF of a metric for its soft-decision decoding. Moreover then, we will use it to define the worst-case coverage probability of the underlying OFDMA network when a convolutional code is employed as an ECC. This method may be applicable to any binary ECC under maximum-likelihood (ML) decoding.

It is well-known in [15] that the BER of a convolutional code is upper bounded by

$$P_{\mathrm{b}} \leq \sum_{d=d_{\mathrm{free}}}^{\infty} B_d P_d$$

where d_{free} is the free distance of the considered convolutional code, B_d denotes the total number of non-zero information bits on all the weight-d paths, divided by the number of information bits per unit time, and P_d stands for the pairwise error probability that a path of weight d is selected as a decoder output, assuming that the all-zero codeword was transmitted.

To compute the pairwise error probability P_d, we can assume without loss of generality that the path chosen by the ML decoder is different from the all-zero path at bit position i, $i = 1, \ldots, d$, and the metrics of the corresponding bits, denoted by L_i, $i = 1, \ldots, d$, are i.i.d. LLRs having the same distribution as a given metric L. Then, P_d can be expressed in [16] as

$$P_d = P\left(\sum_{i=1}^{d} L_i < 0\right). \tag{3}$$

Since it is not easy to evaluate (3) directly, we employ the saddlepoint approximation that approximates the cumulative distribution function (CDF) of the sum of d i.i.d. RVs via the MGF of L as follows. Let $\Phi(s)$ be the MGF of L, defined by $\Phi(s) = \mathbb{E}(\exp(sL))$, and let $\hat{s}$ be the solution to $\Phi^{(1)}(\hat{s}) = 0$, where $\Phi^{(n)}(s) \triangleq (d^n/ds^n)\Phi(s)$. Then, from the saddlepoint approximation in [17], we have

$$P_d \simeq 1 - Q(r) + \frac{1}{\sqrt{2\pi}} \exp\left(-\frac{r^2}{2}\right)\left(\frac{1}{r} - \frac{1}{q}\right) \tag{4}$$

where

$$Q(x) \triangleq \frac{1}{\sqrt{2\pi}}\int_x^\infty \exp\left(-\frac{y^2}{2}\right)\mathrm{d}y,$$
$$r = \mathrm{sgn}(\hat{s})\sqrt{-2d\ \ln\ \Phi(\hat{s})},$$
$$q = \hat{s}\sqrt{d\frac{\Phi^{(2)}(\hat{s})}{\Phi(\hat{s})}},$$

and $\mathrm{sgn}(x)$ denotes the sign of x. This method yields an extremely accurate approximation to the CDF [17].

The coverage probability of the underlying OFDMA network is defined as

$$P_{\text{coverage}} \triangleq P\left(P_{\text{b}}^{L} < P_{\text{b}}^{\text{T}}\right) \tag{5}$$

as in [7]. Here, P_{b}^{L} is the BER when the ECC employed in the underlying OFDMA network is decoded with a given metric L, and P_{b}^{T} denotes the maximum tolerable BER for a data traffic. Unfortunately, it seems very difficult to predict the exact BER performance of the underlying OFDMA network even when a convolutional code is employed as an ECC. Therefore, in this paper, we consider only the *worst-case coverage probability*, that is, the coverage probability when P_{b}^{L} in (5) is replaced by the union bound defined as

$$P_{\text{b, UB}} \triangleq \sum_{d=d_{\text{free}}}^{\infty} B_d P_d. \tag{6}$$

To compute this coverage probability, it is required to derive the MGF of a given metric for soft-decision decoding, which determines the pairwise error probability via (4) and the union bound in (6) in turn.

4 MGFs of the Gaussian and Laplacian Metrics

In this section, we will derive the MGFs of the GM and the LM for soft-decision decoding of the ECC employed in the underlying OFDMA network with QPSK modulation or 16-QAM in order to compute the pairwise error probability P_d in (4). Note that P_d is employed in turn in the computation of the union bound on the BER of a BICM system, and the coverage probability of the underlying OFDMA network is evaluated.

For simplicity, it is assumed that the phase of $H_{\hat{m}}[k]$ is perfectly compensated. Compensated by the phase of $H_{\hat{m}}[k]$, the normalised FFT output in (1) is replaced by

$$\tilde{Y}[k] = |H_{\hat{m}}[k]|c_{\hat{m},k} + \tilde{Z}[k]$$

for $k \in C_{\hat{m}}$, where $\tilde{Y}[k]$ and $\tilde{Z}[k]$ are the phase-compensated signals of $Y[k]$ and $Z[k]$ in (1), respectively.

4.1 Gaussian metric

The legacy GM for soft-decision decoders with QAM over AWGN or Rayleigh fading channels was first introduced in [12]. In general, the GM is the most widely used metric obtained by approximating the real and imaginary parts of $\tilde{Z}[k]$ as i.i.d. Gaussian RVs [18, 19]. For $\nu = 1, \ldots, \log_2 M$, let $L^{\text{GM},\nu}$ be the GM of the νth bit, b_ν belonging to the M-QAM symbol on the kth subcarrier in the underlying OFDMA network. It is given in [10] by (see equation (7)) where A_i^ν denotes the set of the M-QAM symbols whose νth bit is equal to $i \in \{0,\ 1\}$, $\alpha \triangleq |H_{\hat{m}}[k]|$ is a Rayleigh-distributed RV with scale parameter 1/2, $\mathrm{Re}\{x\}$ and $\mathrm{Im}\{x\}$ denote the real and imaginary parts of x, respectively, and

$$\bar{\Upsilon}_{I,\lambda} \triangleq \mathbb{E}\left(|\tilde{Z}[k]|^2|\boldsymbol{I},\ \lambda\right) = \lambda \sum_{m=1, m\neq\hat{m}}^{N_B} I_m + \frac{N_0}{E_{\text{s},\hat{m}}}.$$

Under the Gray-coded bit-to-symbol mapping rule in [20], it suffices to consider only the GMs belonging to the real part of an M-QAM symbol. Moreover, note that the max-log approximation $\ln(e^x + e^y) \simeq \max(x,\ y)$ is widely used in the literature [13, 21], since it lowers the computational load without a serious performance loss. For $\nu = 1, \ldots, (\log_2 M)/2$, let $L_{\text{A},M}^{\text{GM},\nu}$ be the *approximated GM* of the νth bit belonging to the real part of the M-QAM symbol on the kth subcarrier by the max-log approximation. Then

$$L_{\text{A},M}^{\text{GM},\nu} = \min_{\tilde{c}\in B_1^\nu}(\tilde{Y}_{\text{R}}[k] - \alpha\tilde{c})^2 - \min_{\tilde{c}\in B_0^\nu}(\tilde{Y}_{\text{R}}[k] - \alpha\tilde{c})^2 \tag{8}$$

where $\tilde{Y}_{\text{R}}[k]$ is the real part of $\tilde{Y}[k]$ and B_i^ν denotes the set of the real parts of the M-QAM symbols whose νth bit is equal to $i \in \{0,\ 1\}$. For QPSK modulation (or 4-QAM),

$$L_{\text{A},4}^{\text{GM},1} = (\tilde{Y}_{\text{R}}[k] + \alpha\omega_4)^2 - (\tilde{Y}_{\text{R}}[k] - \alpha\omega_4)^2 = 4\alpha\omega_4\tilde{Y}_{\text{R}}[k] \tag{9}$$

where $\omega_4 \triangleq 1/\sqrt{2}$ is the normalisation factor of the QPSK signal energy. Similarly, for 16-QAM,

$$\begin{aligned} L_{\text{A},16}^{\text{GM},1} &= \min_{\tilde{c}\in B_1^1}(\tilde{Y}_{\text{R}}[k] - \alpha\tilde{c})^2 - \min_{\tilde{c}\in B_0^1}(\tilde{Y}_{\text{R}}[k] - \alpha\tilde{c})^2 \\ &= \begin{cases} 8\alpha\omega_{16}\tilde{Y}_{\text{R}}[k] + 8\alpha^2\omega_{16}^2, & \tilde{Y}_{\text{R}}[k] < -2\alpha\omega_{16} \\ 4\alpha\omega_{16}\tilde{Y}_{\text{R}}[k], & -2\alpha\omega_{16} \le \tilde{Y}_{\text{R}}[k] < 2\alpha\omega_{16} \\ 8\alpha\omega_{16}\tilde{Y}_{\text{R}}[k] - 8\alpha^2\omega_{16}^2, & \tilde{Y}_{\text{R}}[k] \ge 2\alpha\omega_{16}, \end{cases} \\ L_{\text{A},16}^{\text{GM},2} &= \min_{\tilde{c}\in B_1^2}(\tilde{Y}_{\text{R}}[k] - \alpha\tilde{c})^2 - \min_{\tilde{c}\in B_0^2}(\tilde{Y}_{\text{R}}[k] - \alpha\tilde{c})^2 \\ &= \begin{cases} 4\alpha\omega_{16}\tilde{Y}_{\text{R}}[k] + 8\alpha^2\omega_{16}^2, & \tilde{Y}_{\text{R}}[k] < 0 \\ -4\alpha\omega_{16}\tilde{Y}_{\text{R}}[k] + 8\alpha^2\omega_{16}^2, & \tilde{Y}_{\text{R}}[k] \ge 0 \end{cases} \end{aligned}$$

where $\omega_{16} \triangleq 1/\sqrt{10}$ is the normalisation factor of the 16-QAM signal energy.

To estimate the upper bound on the BER of the desired MS in the underlying OFDMA network employing the GM, we will derive the MGF $\Phi_M^{\text{GM}}(s|b=0,\ \boldsymbol{I},\ \lambda)$ of the approximated GM of an arbitrary coded-bit, b for M-QAM, conditioned on $b=0$, $\boldsymbol{I}$ and λ. These MGFs are needed in the computation of the pairwise error probability, assuming that the all-zero codeword was transmitted. Since $L_{\text{A},M}^{\text{GM},\nu}$ is a function of α and $\tilde{Y}_{\text{R}}[k]$, it is possible to derive its conditional MGF when the conditional PDF of $\tilde{Y}_{\text{R}}[k]$ is given. Note that

$$\begin{aligned} f_{\tilde{Y}_{\text{R}}[k]}(y|b_\nu = i,\ \alpha,\ \boldsymbol{I},\ \lambda) &= \frac{1}{|B_i^\nu|}\sum_{\tilde{c}\in B_i^\nu} f_{\tilde{Y}_{\text{R}}[k]}(y|\tilde{c},\ \alpha,\ \boldsymbol{I},\ \lambda) \\ &= \frac{1}{|B_i^\nu|}\sum_{\tilde{c}\in B_i^\nu} f_{\tilde{Z}_{\text{R}}[k]}(y - \alpha\tilde{c}|\boldsymbol{I},\ \lambda) \end{aligned} \tag{10}$$

for $i \in \{0,\ 1\}$, where $\tilde{Z}_{\text{R}}[k]$ denotes the real part of $\tilde{Z}[k]$ and

$$L^{\text{GM},\nu} \triangleq \ln\frac{\sum_{c\in A_0^\nu}\exp\left(-\left(\left(\mathrm{Re}\{\tilde{Y}[k] - \alpha c\}\right)^2 + \left(\mathrm{Im}\{\tilde{Y}[k] - \alpha c\}\right)^2\right)/\bar{\Upsilon}_{I,\lambda}\right)}{\sum_{c\in A_1^\nu}\exp\left(-\left(\left(\mathrm{Re}\{\tilde{Y}[k] - \alpha c\}\right)^2 + \left(\mathrm{Im}\{\tilde{Y}[k] - \alpha c\}\right)^2\right)/\bar{\Upsilon}_{I,\lambda}\right)} \tag{7}$$

IET Commun., 2016, Vol. 10, Iss. 1, pp. 24–33

$f_{\tilde{Z}_R[k]}(z|\boldsymbol{I},\ \lambda)$ is given in [10] by

$$f_{\tilde{Z}_R[k]}(z|\boldsymbol{I},\ \lambda)=\sum_{p_{1,k}=0}^{1}\cdots\sum_{p_{\hat{m}-1,k}=0}^{1}\sum_{p_{\hat{m}+1,k}=0}^{1}\cdots\sum_{p_{N_B,k}=0}^{1}\frac{\prod_{m=1,m\neq\hat{m}}^{N_B}((1-\lambda)(1-p_{m,k})+\lambda p_{m,k})}{\sqrt{\pi\Upsilon_{P_k,I,\lambda}}}\times\exp\left(-\frac{z^2}{\Upsilon_{P_k,I,\lambda}}\right).$$

For QPSK modulation, the MGF of the approximated GM, conditioned on $b_1=0$, α, $\boldsymbol{I}$, and λ, can be derived from (9) and (10) as

$$\begin{aligned}&\Phi_4^{\mathrm{GM}}(s|b_1=0,\alpha,\boldsymbol{I},\lambda)\\&=\mathbb{E}\left(\exp\left(sL_{\mathrm{A},4}^{\mathrm{GM},1}\right)\right)\\&=\int_{-\infty}^{\infty}\exp(4\alpha\omega_4 ys)f_{\tilde{Y}_R[k]}(y|b_1=0,\alpha,\boldsymbol{I},\lambda)\mathrm{d}y\\&=\sum_{p_{1,k}=0}^{1}\cdots\sum_{p_{\hat{m}-1,k}=0}^{1}\sum_{p_{\hat{m}+1,k}=0}^{1}\cdots\sum_{p_{N_B,k}=0}^{1}\prod_{m=1,m\neq\hat{m}}^{N_B}((1-\lambda)(1-p_{m,k})+\lambda p_{m,k})\\&\cdot\exp(4\alpha^2\omega_4^2 s(1+\Upsilon_{P_k,I,\lambda}s)).\end{aligned}\tag{11}$$

Averaging $\Phi_4^{\mathrm{GM}}(s|b_1=0,\ \alpha,\ \boldsymbol{I},\ \lambda)$ in (11) over α, we get

$$\begin{aligned}&\Phi_4^{\mathrm{GM}}(s|b_1=0,\ \boldsymbol{I},\ \lambda)\\&=\int_0^{\infty}\Phi_4^{\mathrm{GM}}(s|b_1=0,\ \alpha,\ \boldsymbol{I},\ \lambda)\cdot 2\alpha\exp(-\alpha^2)\mathrm{d}\alpha\\&=\sum_{p_{1,k}=0}^{1}\cdots\sum_{p_{\hat{m}-1,k}=0}^{1}\sum_{p_{\hat{m}+1,k}=0}^{1}\cdots\sum_{p_{N_B,k}=0}^{1}\prod_{m=1,m\neq\hat{m}}^{N_B}\\&\quad((1-\lambda)(1-p_{m,k})+\lambda p_{m,k})\\&\cdot 2g(s;\ \Upsilon_{P_k,I,\lambda},\ \omega_4;\ 4,\ 1,\ 0,\ 0,\ 0,\ 0)\end{aligned}\tag{12}$$

where (13) for positive numbers Υ, ω and integers c_i satisfying $c_1\omega^2 s(c_2+\Upsilon s)<1$, $\Upsilon+\omega^2(c_3+c_4\Upsilon s)>0$ and $c_5+c_6\Upsilon s\geq 0$.

In a similar way, the MGF $\Phi_{16}^{\mathrm{GM},\nu}(s|b_\nu=0,\ \boldsymbol{I},\ \lambda)$ of $L_{\mathrm{A},16}^{\mathrm{GM},\nu}$, $\nu=1,\ 2$ for 16-QAM, conditioned on $b_\nu=0$, $\boldsymbol{I}$ and λ, may be computed as

$$\Phi_{16}^{\mathrm{GM},\nu}(s|b_\nu=0,\ \boldsymbol{I},\ \lambda)=\int_0^{\infty}\mathbb{E}\left(\exp\left(sL_{\mathrm{A},16}^{\mathrm{GM},\nu}\right)\right)\cdot 2\alpha\ \exp(-\alpha^2)\mathrm{d}\alpha,\quad\nu=1,\ 2.$$

See Appendix 1 for more details. Note that the coded bits are assumed to be randomly bit-interleaved in the underlying OFDMA network with 16-QAM and then are mapped to 16-QAM symbols. This implies that the approximated GM, $L_{\mathrm{A},16}^{\mathrm{GM}}$ of an arbitrary coded-bit, b for 16-QAM may be modelled as

$$L_{\mathrm{A},16}^{\mathrm{GM}}=\begin{cases}L_{\mathrm{A},16}^{\mathrm{GM},1}, & \text{with probability } 1/2\\ L_{\mathrm{A},16}^{\mathrm{GM},2}, & \text{with probability } 1/2.\end{cases}\tag{14}$$

Hence, the conditional MGF of $L_{\mathrm{A},16}^{\mathrm{GM}}$ for 16-QAM can be expressed as a mixture form, given by

$$\Phi_{16}^{\mathrm{GM}}(s|b=0,\ \boldsymbol{I},\ \lambda)=\frac{1}{2}\Phi_{16}^{\mathrm{GM},1}(s|b_1=0,\ \boldsymbol{I},\ \lambda)+\frac{1}{2}\Phi_{16}^{\mathrm{GM},2}(s|b_2=0,\ \boldsymbol{I},\ \lambda).\tag{15}$$

4.2 Laplacian metric

As shown in [10], the distribution of $\tilde{Z}[k]$ possesses a heavy tail and deviates significantly from the Gaussian distribution for moderate-to-small cell loads. The results in [10] show that the generalised GM (GGM) obtained by approximating the real and imaginary parts of $\tilde{Z}[k]$ as i.i.d. generalised Gaussian RVs has significantly enhanced performance, compared with the GM. The PDF of a generalised Gaussian RV X is given in [22] by

$$f_X(x)=\frac{a_1}{2a_2\Gamma(1/a_1)}\exp\left(-\left(\frac{|x|}{a_2}\right)^{a_1}\right)\tag{16}$$

where a_1 is the shape parameter determined by the normalised kurtosis of X, a_2 is the scaling factor given by $a_2=\sqrt{\Gamma(1/a_1)/\Gamma(3/a_1)\mathbb{E}(X^2)}$, and $\Gamma(z)\triangleq\int_0^{\infty}t^{z-1}\exp(-t)\,\mathrm{d}t$ [23]. The RV X is Laplacian for $a_1=1$, whereas it is Gaussian for $a_1=2$ [24]. In general, the shape parameter a_1 in (16) makes it very difficult to derive the MGF of the GGM and analyse the corresponding coverage probability of downlink subcarrier-hopping cellular OFDMA networks, except for the case that $a_1=1$ or 2. This is why we employ the GGM with $a_1=1$ as a simple non-GM in this paper.

Approximating the real and imaginary parts of $\tilde{Z}[k]$ as i.i.d. Laplacian RVs, that is, $a_1=1$ in (16), we define the LM for soft-decision decoding of an employed ECC. The LM has little performance loss for QPSK modulation, compared with the GGM. Even though the LM for 16-QAM exhibits slightly worse performance than the GGM, it still outperforms the GM for moderate-to-small cell loads. For $\nu=1,\ \ldots,\ \log_2 M$, let $L^{\mathrm{LM},\nu}$ be the LM of the νth bit belonging to the M-QAM symbol on the kth subcarrier in the underlying OFDMA network, given by (17) where $\bar{\Upsilon}_{\boldsymbol{I},\lambda}$, A_i^{ν} and α are defined as before. As in the GM, let $L_{\mathrm{A},M}^{\mathrm{LM},\nu}$, $\nu=1,\ \ldots,\ (\log_2 M)/2$ be the *approximated LM* of the νth bit belonging to the real part of the M-QAM symbol on the kth subcarrier by the max-log approximation. Then

$$L_{\mathrm{A},M}^{\mathrm{LM},\nu}=\min_{\tilde{c}\in B_1^{\nu}}|\tilde{Y}_R[k]-\alpha\tilde{c}|-\min_{\tilde{c}\in B_0^{\nu}}|\tilde{Y}_R[k]-\alpha\tilde{c}|$$

$$(s;\ \Upsilon,\ \omega;\ c_1,\ c_2,\ c_3,\ c_4,\ c_5,\ c_6)\triangleq\frac{\omega(c_5+c_6\Upsilon s)-\sqrt{\Upsilon+\omega^2(c_3+c_4\Upsilon s)}}{2(-1+c_1\omega^2 s(c_2+\Upsilon s))\sqrt{\Upsilon+\omega^2(c_3+c_4\Upsilon s)}}\tag{13}$$

$$L^{\mathrm{LM},\nu}=\ln\frac{\sum_{c\in A_0^{\nu}}\exp\left(-\left(|\mathrm{Re}\{\tilde{Y}[k]-\alpha c\}|+|\mathrm{Im}\{\tilde{Y}[k]-\alpha c\}|\right)/\sqrt{\bar{\Upsilon}_{I,\lambda}/4}\right)}{\sum_{c\in A_1^{\nu}}\exp\left(-\left(|\mathrm{Re}\{\tilde{Y}[k]-\alpha c\}|+|\mathrm{Im}\{\tilde{Y}[k]-\alpha c\}|\right)/\sqrt{\bar{\Upsilon}_{I,\lambda}/4}\right)}\tag{17}$$

where $\tilde{Y}_{\mathrm{R}}[k]$ and B_i^v are defined as in (8). For QPSK modulation,

$$L_{\mathrm{A},4}^{\mathrm{LM},1} = |\tilde{Y}_{\mathrm{R}}[k] + \alpha\omega_4| - |\tilde{Y}_{\mathrm{R}}[k] - \alpha\omega_4| = \begin{cases} -2\alpha\omega_4, & \tilde{Y}_{\mathrm{R}}[k] < -\alpha\omega_4 \\ 2\tilde{Y}_{\mathrm{R}}[k], & -\alpha\omega_4 \le \tilde{Y}_{\mathrm{R}}[k] < \alpha\omega_4 \\ 2\alpha\omega_4, & \tilde{Y}_{\mathrm{R}}[k] \ge \alpha\omega_4 \end{cases} \quad (18)$$

where $\omega_4 = 1/\sqrt{2}$. Similarly, for 16-QAM,

$$L_{\mathrm{A},16}^{\mathrm{LM},1} = \min_{\tilde{c}\in B_1^1} |\tilde{Y}_{\mathrm{R}}[k] - \alpha\tilde{c}| - \min_{\tilde{c}\in B_0^1} |\tilde{Y}_{\mathrm{R}}[k] - \alpha\tilde{c}| = \begin{cases} -4\alpha\omega_{16}, & \tilde{Y}_{\mathrm{R}}[k] < -3\alpha\omega_{16} \\ 2\tilde{Y}_{\mathrm{R}}[k] + 2\alpha\omega_{16}, & -3\alpha\omega_{16} \le \tilde{Y}_{\mathrm{R}}[k] < -2\alpha\omega_{16} \\ -2\alpha\omega_{16}, & -2\alpha\omega_{16} \le \tilde{Y}_{\mathrm{R}}[k] < -\alpha\omega_{16} \\ 2\tilde{Y}_{\mathrm{R}}[k], & -\alpha\omega_{16} \le \tilde{Y}_{\mathrm{R}}[k] < \alpha\omega_{16} \\ 2\alpha\omega_{16}, & \alpha\omega_{16} \le \tilde{Y}_{\mathrm{R}}[k] < 2\alpha\omega_{16} \\ 2\tilde{Y}_{\mathrm{R}}[k] - 2\alpha\omega_{16}, & 2\alpha\omega_{16} \le \tilde{Y}_{\mathrm{R}}[k] < 3\alpha\omega_{16} \\ 4\alpha\omega_{16}, & \tilde{Y}_{\mathrm{R}}[k] \ge 3\alpha\omega_{16}, \end{cases}$$

$$L_{\mathrm{A},16}^{\mathrm{LM},2} = \min_{\tilde{c}\in B_1^2} |\tilde{Y}_{\mathrm{R}}[k] - \alpha\tilde{c}| - \min_{\tilde{c}\in B_0^2} |\tilde{Y}_{\mathrm{R}}[k] - \alpha\tilde{c}| = \begin{cases} -2\alpha\omega_{16}, & \tilde{Y}_{\mathrm{R}}[k] < -3\alpha\omega_{16} \\ 2\tilde{Y}_{\mathrm{R}}[k] + 4\alpha\omega_{16}, & -3\alpha\omega_{16} \le \tilde{Y}_{\mathrm{R}}[k] < -\alpha\omega_{16} \\ 2\alpha\omega_{16}, & -\alpha\omega_{16} \le \tilde{Y}_{\mathrm{R}}[k] < \alpha\omega_{16} \\ -2\tilde{Y}_{\mathrm{R}}[k] + 4\alpha\omega_{16}, & \alpha\omega_{16} \le \tilde{Y}_{\mathrm{R}}[k] < 3\alpha\omega_{16} \\ -2\alpha\omega_{16}, & \tilde{Y}_{\mathrm{R}}[k] \ge 3\alpha\omega_{16} \end{cases}$$

where $\omega_{16} = 1/\sqrt{10}$.

Using the same approach as in the GM case of the previous section, we will derive the MGF $\Phi_M^{\mathrm{LM}}(s|b=0, \boldsymbol{I}, \lambda)$ of the approximated LM of an arbitrary coded-bit, b for M-QAM, conditioned on $b=0$, $\boldsymbol{I}$, and λ. It is needed in the estimation of the upper bound on the BER of the desired MS in the underlying OFDMA network employing the LM. For QPSK modulation, the MGF of the approximated LM, conditioned on $b_1 = 0$, $\boldsymbol{I}$, and λ, may be obtained from (18) and (10) as

$$\Phi_4^{\mathrm{LM}}(s|b_1 = 0, \boldsymbol{I}, \lambda) = \int_0^\infty \mathbb{E}\left(\exp\left(sL_{\mathrm{A},4}^{\mathrm{LM},1}\right)\right) \cdot 2\alpha \exp(-\alpha^2)\,\mathrm{d}\alpha. \quad (19)$$

See Appendix 2 for more details.

Similarly, the MGF $\Phi_{16}^{\mathrm{LM},v}(s|b_v = 0, \boldsymbol{I}, \lambda)$ of $L_{\mathrm{A},16}^{\mathrm{LM},v}$, $v = 1, 2$ for 16-QAM, conditioned on $b_v = 0$, $\boldsymbol{I}$ and λ, may be derived. See Appendix 3 for more details. Under the same situation as in the case of the approximated GM, the approximated LM, $L_{\mathrm{A},16}^{\mathrm{LM}}$ of an arbitrary coded-bit, b for 16-QAM may be modelled as

$$L_{\mathrm{A},16}^{\mathrm{LM}} = \begin{cases} L_{\mathrm{A},16}^{\mathrm{LM},1}, & \text{with probability } 1/2 \\ L_{\mathrm{A},16}^{\mathrm{LM},2}, & \text{with probability } 1/2. \end{cases} \quad (20)$$

Hence, the conditional MGF of $L_{\mathrm{A},16}^{\mathrm{LM}}$ for 16-QAM can be expressed as a mixture form, given by

$$\Phi_{16}^{\mathrm{LM}}(s|b=0, \boldsymbol{I}, \lambda) = \frac{1}{2}\Phi_{16}^{\mathrm{LM},1}(s|b_1 = 0, \boldsymbol{I}, \lambda) + \frac{1}{2}\Phi_{16}^{\mathrm{LM},2}(s|b_2 = 0, \boldsymbol{I}, \lambda). \quad (21)$$

5 Numerical results

We present numerical results on the coverage performance of downlink subcarrier-hopping cellular OFDMA networks with QPSK modulation or 16-QAM when the LM or the GM are used for soft-decision decoding of an employed ECC. For our simulation, omnidirectional hexagonal cells are considered with N_B equal to 7. The desired MS is assumed to be located at the cell edge and the noise figure F of the desired MS is set to 7 dB as in [7] with the absolute temperature T of 290 K. The FFT size N is taken to be 1024 and the signal bandwidth W is set to 10 MHz. The average BS transmit power A_{B} is considered to be 5, 10, 20, and 40 W. The shadowing standard deviation σ_{S} is set to 8 dB for the shadowing case and the path loss model is assumed to be $\rho = 128.1$ dB at 1 km with $\mu = 3.76$ as in [7]. The convolutional code with generator polynomials $(175)_8$, $(133)_8$, and $(145)_8$ whose weight spectrum is given in [25] is employed where the information length is 144, the code rate is 1/3, the constraint length is 7, and the Viterbi algorithm is employed for decoding. The coded bits are randomly interleaved prior to being mapped into a stream of QAM symbols.

In the underlying OFDMA network with QPSK modulation, the sum $\sum_{i=1}^{d} L_i$ in (3) consists of d i.i.d. RVs where L_i, $i = 1, \ldots, d$, have the same distribution as $L_{\mathrm{A},4}^{\mathrm{GM},1}$ in (8) for the approximated GM or $L_{\mathrm{A},4}^{\mathrm{LM},1}$ in (18) for the approximated LM. Similarly, in the case of 16-QAM, it is made up of d i.i.d. RVs where L_i, $i = 1, \ldots, d$, have the same distribution as $L_{\mathrm{A},16}^{\mathrm{GM}}$ in (14) or $L_{\mathrm{A},16}^{\mathrm{LM}}$ in (20). The MGFs in (12), (15), (19), and (21) can be applied to the computation of the corresponding pairwise error probability P_d in (4). Since the pairwise error probabilities obtained from the MGFs in (12), (15), (19), and (21) are conditioned on $\boldsymbol{I}$ and λ, the coverage probability conditioned on λ can be computed by averaging the coverage probability in (5) over $\boldsymbol{I}$ via Monte Carlo integration techniques [26].

For the no-shadowing case, the BER of the networks with QPSK modulation or 16-QAM is shown in terms of the cell load in Fig. 1, where the radius of each cell is set to 1 km and the average BS transmit power is set to 20 W. Even though the LM has slightly worse performance than the GGM, it exhibits much better performance than the GM for moderate-to-small cell loads. Moreover, as the cell load decreases, the upper bounds on the BER agree with the simulation results at the range of BER $< 10^{-4}$. Except Fig. 1, we assume the shadowing case throughout this section and compute the coverage probability of the networks for small cell loads. Note that small cell loads are considered to be practical as in [4, 7, 27–29].

Fig. 2 shows the coverage probability versus the cell load. The target BER, $P_{\mathrm{b}}^{\mathrm{T}}$ ranges from 10^{-5} to 10^{-3} [30] for various types of traffic, as shown in Table 1. The radius of each cell is set to 1 km and the average BS transmit power is set to 20 W. For the cell load of $\lambda < 50\%$, the coverage probability for the LM outperforms that for the GM as expected, since the ICI-plus-noise is impulsive for

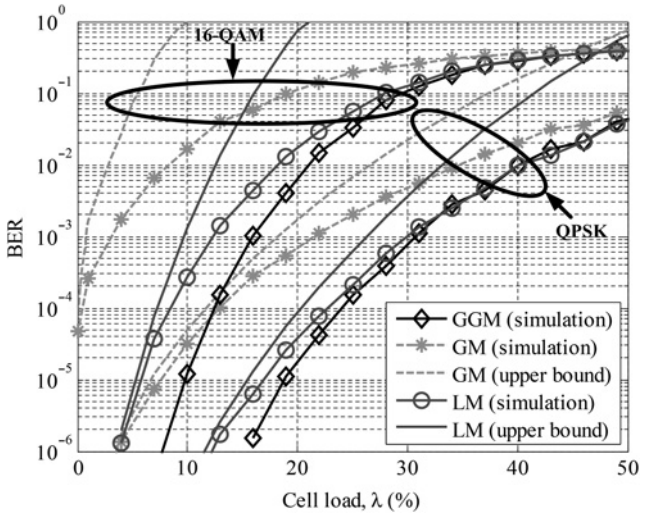

Fig. 1 *BER versus the cell load for the no-shadowing case when $A_B = 20$ W and the cell radius is set to 1 km*

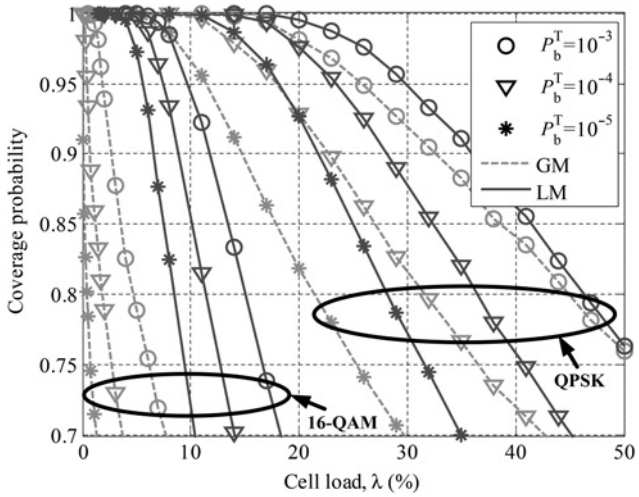

Fig. 2 *Coverage probability versus the cell load when $\sigma_S = 8$ dB, $A_B = 20$ W, and the cell radius is set to 1 km*

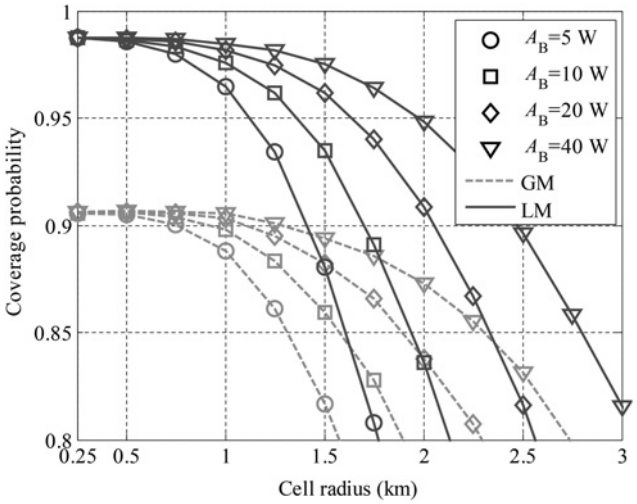

Fig. 4 *Coverage probability versus the cell radius for QPSK modulation when $\sigma_S = 8$ dB and $P_b^T = 10^{-5}$ (λ = 14.8%)*

Table 1 Maximum tolerable BERs for various types of traffic [30]

Types of traffic	Maximum tolerable BER (P_b^T)
voice	10^{-3}
constant bit rate digital audio	10^{-4}
constant bit rate digital video	10^{-5}

moderate-to-small cell loads. Moreover, as the target BER decreases, the cell load satisfying the coverage probability of 90% increases when the LM is employed instead of the GM. For example, by employing the LM instead of the GM for 16-QAM, the cell load satisfying the coverage probability of 90% increases from 2.6% to 11.7% at $P_b^T = 10^{-3}$ and from 0.7% to 8.8% at $P_b^T = 10^{-4}$. This is approximately four-fold at $P_b^T = 10^{-3}$ and twelve-fold at $P_b^T = 10^{-4}$.

The coverage probability versus the cell radius is shown in Figs. 3–5. We first choose the values of the cell load from Fig. 2, which satisfy the coverage probability of 90% with the GM. Next, we evaluate the coverage probability versus the cell radius for a given value of the cell load when the average BS transmit power varies. The expected gain in the cell radius of networks satisfying the coverage probability of 90% increases by at least 40% and 180% for QPSK modulation and 16-QAM, respectively, when the LM is employed instead of the GM. Moreover, the average BS transmit power can be reduced by at least 6 dB for all the considered cases when the LM is employed instead of the GM. For example, in Fig. 3, the cell radius of the networks satisfying the coverage probability of 90% with the GM and $A_B = 20$ W is the same as that of the networks with the LM and $A_B = 5$ W. The gain in the achievable cell radius and the amount of the average BS transmit power reduction may be further improved if the GGM is employed instead of the LM.

In the case of high cell loads, the distribution of the ICI-plus-noise is observed in [10, 11] to be close to the Gaussian distribution. Thus, we can easily expect without the help of analysis that the networks employing the LM or the GGM may have almost the same coverage performance as those employing the GM for high cell loads. In fact, Fig. 1 shows that these two networks tend to have the same BER performance when the cell loads increase.

6 Conclusions

We analysed the coverage performance of downlink subcarrier-hopping cellular OFDMA networks with QPSK modulation or 16-ary QAM, based on the union bound on the BER of a BICM system. The MGFs for the GM and the LM were derived and used for computing the pairwise error probability and

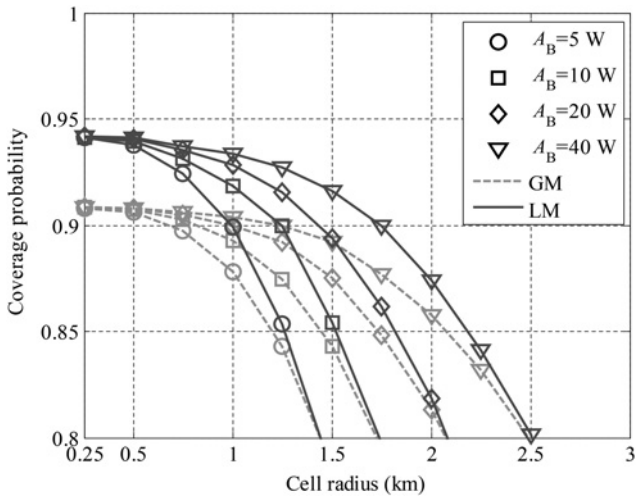

Fig. 3 *Coverage probability versus the cell radius for QPSK modulation when $\sigma_S = 8$ dB and $P_b^T = 10^{-3}$ (λ = 32.7%)*

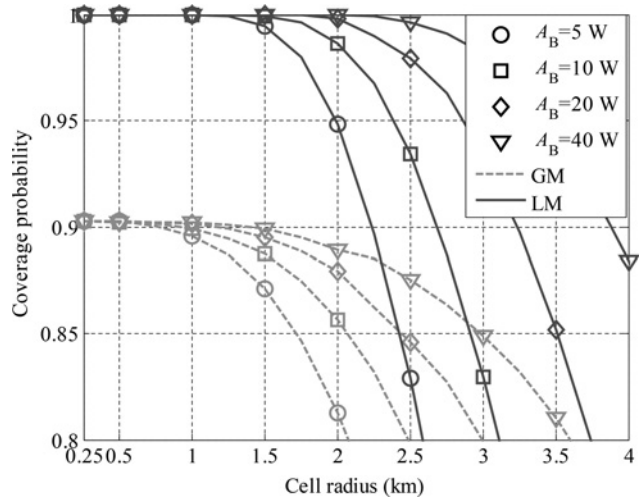

Fig. 5 *Coverage probability versus the cell radius for 16-QAM when $\sigma_S = 8$ dB and $P_b^T = 10^{-3}$ (λ = 2.6%)*

the coverage probability when a convolutional code is employed. Numerical results demonstrate that downlink subcarrier-hopping cellular OFDMA networks with the LM significantly outperform those with the GM in terms of the achievable cell radius and the amount of the average BS transmit power reduction when the cell loads are moderate to small. It is also expected that the coverage performance may be further improved with a non-GM that outperforms the LM. Furthermore, our approach can be naturally extended to the cases of 64-ary or 256-ary QAM, even though these cases are not included here due to the limit of space.

7 Acknowledgments

This research was supported in part by the National Research Foundation (NRF) of Korea under grant 2011-0017396 funded by the Ministry of Science, Information and Communication Technology (ICT) and Future Planning (MSIP) of the Korea Government and in part by the MSIP, under the Information Technology Research Center (ITRC) support programme IITP-2015-H8501-15-1006 supervised by the Institute for Information and Communications Technology Promotion (IITP).

8 References

1 IEEE P802.16e/D12: 'Part 16: Air interface for fixed and mobile broadband wireless access systems', 2007
2 IEEE P802.16m/D10: 'Part 16: Air interface for broadband wireless access systems-advanced air interface', 2010
3 3GPP LTE: 'Technical specification group radio access network; evolved universal terrestrial radio access (E-UTRA); physical channels and modulation (Release 10)', 2011
4 Cavers, J.K.: 'Mobile channel characteristics' (Kluwer Academic, 2000, 1st edn.)
5 Sternad, M., Ottosson, T., Ahlen, A., *et al.*: 'Attaining both coverage and high spectral efficiency with adaptive OFDM downlinks'. Proc. IEEE Vehicular Technology Conf., Orlando, USA, October 2003, pp. 2486–2490
6 Lee, W., Nguyen, M.V., Lee, H.S.: 'A resource allocation algorithm and system architecture to extend the cell coverage and alleviate the inter-cell interference'. Proc. IEEE Symp. on Computers and Communications, Marrakech, Morocco, July 2008, pp. 222–227
7 Jalloul, L.M.A., Alex, S.P.: 'Coverage analysis for IEEE 802.16e/WiMAX systems', *IEEE Trans. Wirel. Commun.*, 2008, **7**, (11), pp. 4627–4634
8 Joshi, G., Karandikar, A.: 'Optimal relay placement for cellular coverage extension'. Proc. IEEE National Conf. on Communications, Bangalore, India, January 2011, pp. 1–5
9 Viterbi, A.J., Viterbi, A.M., Gilhousen, K.S., *et al.*: 'Soft handoff extends CDMA cell coverage and increases reverse link capacity', *IEEE J. Sel. Areas Commun.*, 1994, **12**, (8), pp. 1281–1288
10 Seol, C., Cheun, K.: 'A statistical inter-cell interference model for downlink cellular OFDMA networks under log-normal shadowing and multipath Rayleigh fading', *IEEE Trans. Commun.*, 2009, **57**, (10), pp. 3069–3077
11 Seol, C., Cheun, K., Hong, S.: 'A statistical inter-cell interference model for downlink cellular OFDMA networks under log-normal shadowing with Ricean fading', *IEEE Commun. Lett.*, 2010, **14**, (11), pp. 1011–1013
12 LeGoff, S., Glavieux, A., Berrou, C.: 'Turbo-codes and high spectral efficiency modulation'. Proc. IEEE Int. Conf. on Communications, New Orleans, USA, May 1994, pp. 645–649
13 Szczecinski, L., Alvarado, A., Feick, R.: 'Distribution of max-log metrics for QAM-based BICM in fading channels', *IEEE Trans. Commun.*, 2009, **57**, (9), pp. 2558–2563
14 Haykin, S.: 'Communication systems' (John Wiley & Sons, 2001, 4th edn.)
15 Viterbi, A.J.: 'Convolutional codes and their performance in communication systems', *IEEE Trans. Commun.*, 1971, **COM-19**, (5), pp. 751–772
16 Martinez, A., Fabregas, A.G., Caire, G.: 'Error probability analysis of bit-interleaved coded modulation', *IEEE Trans. Inf. Theory*, 2006, **52**, (1), pp. 262–271
17 Huzurbazar, S.: 'Practical saddlepoint approximations', *Am. Stat.*, 1999, **53**, (3), pp. 225–232
18 Li, J., Kim, H., Lee, Y., *et al.*: 'A novel broadband wireless OFDMA scheme for downlink in cellular communications'. Proc. IEEE Wireless Communications and Networking Conf., New Orleans, USA, March 2003, pp. 1907–1911
19 Elayoubi, S., Fourestie, B., Auffret, X.: 'On the capacity of OFDMA 802.16 systems'. Proc. IEEE Int. Conf. on Communications, Istanbul, Turkey, June 2006, pp. 1760–1765
20 Agrell, E., Lassing, J., Strom, E.G., *et al.*: 'Gray coding for multilevel constellations in Gaussian noise', *IEEE Trans. Inf. Theory*, 2007, **53**, (1), pp. 224–235
21 Viterbi, A.J.: 'An intuitive justification and a simplified implementation of the MAP decoder for convolutional codes', *IEEE J. Sel. Areas Commun.*, 1998, **16**, (2), pp. 260–264
22 Teschioni, A., Sacchi, C., Regazzoni, C.: 'Non-Gaussian characterization of DS/CDMA noise in few-user systems with complex signature sequences', *IEEE Trans. Signal Process.*, 1999, **47**, (1), pp. 234–237
23 Proakis, J.G.: 'Digital communications' (McGraw-Hill, 2000, 4th edn.)
24 Papoulis, A., Pillai, S.U.: 'Probability, random variables and stochastic processes' (McGraw-Hill, 2002, 4th edn.)
25 Conan, J.: 'The weight spectra of some short low-rate convolutional codes', *IEEE Trans. Commun.*, 1984, **32**, (9), pp. 1050–1053
26 Gardner, F.M., Baker, J.D.: 'Simulation techniques: models of communication signal and processes' (New York: Wiley, 1995, 1st edn.)
27 Love, R., Ghosh, A., Classon, B.: 'Downlink control channel design for 3GPP LTE'. Proc. IEEE Wireless Communications and Networking Conf., Las Vegas, USA, March 2008, pp. 813–818
28 Tan, W.L., Lam, F., Lau, W.C.: 'An empirical study on the capacity and performance of 3G networks', *IEEE Trans. Mob. Comput.*, 2008, **7**, (6), pp. 717–750
29 Kumar, S., Monghal, G., Nin, J., *et al.*: 'Autonomous inter cell interference avoidance under fractional load for downlink long term evolution'. Proc. IEEE Vehicular Technology Conf., Barcelona, Spain, April 2009, pp. 1–5
30 Akyildiz, I.F., Levine, D.A., Joe, I.: 'A slotted CDMA protocol with BER scheduling for wireless multimedia networks', *IEEE/ACM Trans. Netw.*, 1999, **7**, (2), pp. 146–158
31 Chiani, M., Dardari, D., Simon, M.K.: 'New exponential bounds and approximations for the computation of error probability in fading channels', *IEEE Trans. Wirel. Commun.*, 2003, **2**, (4), pp. 840–845
32 Renzo, M.D., Graziosi, F., Santucci, F.: 'A unified framework for performance analysis of CSI-assisted cooperative communications over fading channels', *IEEE Trans. Commun.*, 2009, **57**, (9), pp. 2551–2557
33 Shen, Y., Wymeersch, H., Win, M.Z.: 'Fundamental limits of wideband localization-part II: cooperative networks', *IEEE Trans. Inf. Theory*, 2010, **56**, (10), pp. 4981–5000
34 Basar, E., Aygolu, U., Panayirci, E., *et al.*: 'Orthogonal frequency division multiplexing with index modulation', *IEEE Trans. Signal Process.*, 2013, **61**, (22), pp. 5536–5549

9 Appendices

9.1 Appendix 1: Derivation of the MGF of $L_{A,16}^{GM,\nu}$, $\nu = 1, 2$ for 16-QAM

The expressions for the MGF of $L_{A,16}^{GM,\nu}$, $\nu = 1, 2$ for 16-QAM may be derived as (see equation (22))

and (see equation (23))

9.2 Appendix 2: derivation of the MGF $\Phi_4^{LM}(s|b_1 = 0, \boldsymbol{I}, \lambda)$ of $L_{A,4}^{LM,1}$ for QPSK modulation

The MGF of $L_{A,4}^{LM,1}$ may be obtained from (18) and (10) as (see equation (24)) where

$$\phi_1(x) \triangleq 1 + 2\exp(x^2)Q(x\sqrt{2}).$$

Since there is no closed-form expression for $Q(x)$, we employ the approximation of $Q(x)$ given in [31] by

$$Q(x) \simeq \begin{cases} \frac{1}{12}\exp\left(-\frac{x^2}{2}\right) + \frac{1}{4}\exp\left(-\frac{2x^2}{3}\right), & x \geq 0 \\ 1 - \left[\frac{1}{12}\exp\left(-\frac{x^2}{2}\right) + \frac{1}{4}\exp\left(-\frac{2x^2}{3}\right)\right], & x < 0. \end{cases} \tag{25}$$

Note that this approximation provides a tight upper bound for $Q(x)$ and is widely used for performance analysis of the system [32–34]. On the basis of this approximation, we may approximate $\Phi_4^{LM}(s|b_1 = 0, \boldsymbol{I}, \lambda)$ in (24) as (see equation (26) at the bottom of the next page) for $s \geq 0$, where

$$\phi_2(x) \triangleq 1 - 2\sqrt{\pi}x\exp(x^2)Q(x\sqrt{2}),$$

$$\zeta(s; \Upsilon, \omega; c_1, c_2, c_3) \triangleq \left(c_1\beta(\Upsilon, \omega; c_2)\right)^{-1}\phi_2\left(c_3\omega s\left(\beta(\Upsilon, \omega; c_2)\right)^{-1/2}\right),$$

$$\beta(\Upsilon, \omega; c_1) \triangleq 1 + c_1\omega^2\Upsilon^{-1}$$

for positive numbers Υ, ω and real numbers c_i. In general, s is a complex variable, while the argument in the Q-function is

restricted to a real number. Therefore, s is dealt with as a real variable here.

When $s<0$, the MGF $\Phi_4^{\mathrm{LM}}(s|b_1=0,\ \boldsymbol{I},\ \lambda)$ of $L_{\mathrm{A},4}^{\mathrm{LM},1}$ can be similarly approximated from (24) by using the approximation of $Q(x)$ in (25), that is (27) where (28) for positive numbers Υ, ω and real numbers c_i.

9.3 Appendix 3: derivation of the MGF of $L_{A,16}^{LM,\nu}$, $\nu=1,2$ for 16-QAM

In this Appendix, the approximated expressions for the MGF of $L_{\mathrm{A},16}^{\mathrm{LM},\nu}$, $\nu=1,2$ for 16-QAM are presented. Using the approximation of $Q(x)$ in (25), we approximate (see (29)) and (30) where (31) for positive numbers Υ, ω and real numbers c_i.

$$
\begin{aligned}
&\Phi_{16}^{\mathrm{GM},1}(s|b_1=0,\ \boldsymbol{I},\ \lambda)\\
&=\int_0^{\infty}\mathbb{E}\left(\exp\left(sL_{\mathrm{A},16}^{\mathrm{GM},1}\right)\right)\cdot 2\alpha\,\exp\left(-\alpha^2\right)\mathrm{d}\alpha\\
&=\sum_{p_{1,k}=0}^{1}\cdots\sum_{p_{\hat{m}-1,k}=0}^{1}\sum_{p_{\hat{m}+1,k}=0}^{1}\cdots\sum_{p_{N_B,k}=0}^{1}\prod_{m=1,m\neq\hat{m}}^{N_B}\left((1-\lambda)(1-p_{m,k})+\lambda p_{m,k}\right)\\
&\quad\cdot\frac{1}{2}\Big\{g(s;\ \Upsilon_{P_k,I,\lambda},\ \omega_{16};\ 16,\ 0,\ 1,\ -8,\ 1,\ -4)+g(s;\ \Upsilon_{P_k,I,\lambda},\ \omega_{16};\ 16,\ 2,\ 25,\ 8,\ 5,\ 4)\\
&\quad+2g(s;\ \Upsilon_{P_k,I,\lambda},\ \omega_{16};\ 4,\ 1,\ 0,\ 0,\ 0,\ 0)-g(s;\ \Upsilon_{P_k,I,\lambda},\ \omega_{16};\ 4,\ 3,\ 25,\ 8,\ 5,\ 2)\\
&\quad+2g(s;\ \Upsilon_{P_k,I,\lambda},\ \omega_{16};\ 16,\ 1,\ 0,\ 0,\ 0,\ 0)-g(s;\ \Upsilon_{P_k,I,\lambda},\ \omega_{16};\ 4,\ 1,\ 9,\ 8,\ 3,\ 2)\\
&\quad+g(s;\ \Upsilon_{P_k,I,\lambda},\ \omega_{16};\ 4,\ 3,\ 1,\ -8,\ 1,\ 2)+g(s;\ \Upsilon_{P_k,I,\lambda},\ \omega_{16};\ 16,\ 1,\ 9,\ 8,\ 3,\ 4)\\
&\quad-g(s;\ \Upsilon_{P_k,I,\lambda},\ \omega_{16};\ 4,\ 1,\ 1,\ -8,\ 1,\ -2)-g(s;\ \Upsilon_{P_k,I,\lambda},\ \omega_{16};\ 16,\ 1,\ 1,\ -8,\ 1,\ 4)\Big\}
\end{aligned}
\tag{22}
$$

$$
\begin{aligned}
&\Phi_{16}^{\mathrm{GM},2}(s|b_2=0,\ \boldsymbol{I},\ \lambda)\\
&=\int_0^{\infty}\mathbb{E}\left(\exp\left(sL_{\mathrm{A},16}^{\mathrm{GM},2}\right)\right)\cdot 2\alpha\,\exp\left(-\alpha^2\right)\mathrm{d}\alpha\\
&=\sum_{p_{1,k}=0}^{1}\cdots\sum_{p_{\hat{m}-1,k}=0}^{1}\sum_{p_{\hat{m}+1,k}=0}^{1}\cdots\sum_{p_{N_B,k}=0}^{1}\prod_{m=1,m\neq\hat{m}}^{N_B}\left((1-\lambda)(1-p_{m,k})+\lambda p_{m,k}\right)\\
&\quad\cdot\Big\{g(s;\ \Upsilon_{P_k,I,\lambda},\ \omega_{16};\ 4,\ 3,\ 1,\ -8,\ 1,\ 2)-g(s;\ \Upsilon_{P_k,I,\lambda},\ \omega_{16};\ 4,\ 1,\ 1,\ -8,\ 1,\ -2)\\
&\quad+2g(s;\ \Upsilon_{P_k,I,\lambda},\ \omega_{16};\ 4,\ 1,\ 0,\ 0,\ 0,\ 0)\Big\}.
\end{aligned}
\tag{23}
$$

$$
\begin{aligned}
&\Phi_4^{\mathrm{LM}}(s|b_1=0,\ \boldsymbol{I},\ \lambda)\\
&=\int_0^{\infty}\mathbb{E}\left(\exp\left(sL_{\mathrm{A},4}^{\mathrm{LM},1}\right)\right)\cdot 2\alpha\,\exp\left(-\alpha^2\right)\mathrm{d}\alpha\\
&=\sum_{p_{1,k}=0}^{1}\cdots\sum_{p_{\hat{m}-1,k}=0}^{1}\sum_{p_{\hat{m}+1,k}=0}^{1}\cdots\sum_{p_{N_B,k}=0}^{1}\prod_{m=1,m\neq\hat{m}}^{N_B}\left((1-\lambda)(1-p_{m,k})+\lambda p_{m,k}\right)\\
&\quad\cdot\int_0^{\infty}\left\{\exp\left(-2\alpha\omega_4 s\right)Q\left(\frac{2\alpha\omega_4}{\sqrt{\Upsilon_{\boldsymbol{P}_k,\boldsymbol{I},\lambda}/2}}\right)+\frac{1}{2}\exp\left(2\alpha\omega_4 s\right)\phi_1\left(s\sqrt{\Upsilon_{P_k,I,\lambda}}\right)\right.\\
&\quad\left.-\exp\left(s^2\Upsilon_{P_k,I,\lambda}+2\alpha\omega_4 s\right)Q\left(\frac{2\alpha\omega_4+s\Upsilon_{P_k,I,\lambda}}{\sqrt{\Upsilon_{P_k,I,\lambda}/2}}\right)\right\}\cdot 2\alpha\,\exp\left(-\alpha^2\right)\mathrm{d}\alpha
\end{aligned}
\tag{24}
$$

$$
\begin{aligned}
\Phi_4^{\mathrm{LM}}(s|b_1=0,\ \boldsymbol{I},\ \lambda)\simeq&\sum_{p_{1,k}=0}^{1}\cdots\sum_{p_{\hat{m}-1,k}=0}^{1}\sum_{p_{\hat{m}+1,k}=0}^{1}\cdots\sum_{p_{N_B,k}=0}^{1}\prod_{m=1,m\neq\hat{m}}^{N_B}\left((1-\lambda)(1-p_{m,k})+\lambda p_{m,k}\right)\\
&\cdot\left\{\zeta\left(s;\ \Upsilon_{P_k,I,\lambda},\ \omega_4;\ 4,\ \frac{16}{3},\ 1\right)+\frac{1}{2}\phi_1\left(s\sqrt{\Upsilon_{P_k,I,\lambda}}\right)\phi_2(-\omega_4 s)\right.\\
&\left.-\exp\left(-\frac{s^2\Upsilon_{P_k,I,\lambda}}{3}\right)\zeta\left(s;\ \Upsilon_{P_k,I,\lambda},\ \omega_4;\ 4,\ \frac{16}{3},\ \frac{5}{3}\right)\right\}
\end{aligned}
\tag{26}
$$

$$\Phi_4^{\mathrm{LM}}(s|b_1=0,\ \boldsymbol{I},\ \lambda)=\int_0^{\infty}\mathbb{E}\Big(\exp\left(sL_{\mathrm{A},4}^{\mathrm{LM},1}\right)\Big)\cdot 2\alpha\,\exp\left(-\alpha^2\right)\mathrm{d}\alpha$$

$$\simeq\sum_{p_{1,k}=0}^{1}\cdots\sum_{p_{\hat{m}-1,k}=0}^{1}\sum_{p_{\hat{m}+1,k}=0}^{1}\cdots\sum_{p_{N_B,k}=0}^{1}\prod_{m=1,\,m\neq\hat{m}}^{N_B}\left((1-\lambda)(1-p_{m,k})+\lambda p_{m,k}\right)$$

$$\cdot\Bigg\{\xi\left(s;\ \Upsilon_{P_k,I,\lambda},\ \omega_4;\ 4,\ 1\right)+\frac{1}{2}\phi_1\Big(s\sqrt{\Upsilon_{P_k,I,\lambda}}\Big)\phi_2(-\omega_4 s)-\exp\Big(\Upsilon_{P_k,I}s^2\Big)\chi\Big(s;\ \Upsilon_{P_k,I},\ \omega_4;\ \frac{1}{2},\ 1\Big)$$

$$-\Big(12\beta(\Upsilon_{P_k,I},\ \omega_4;\ 4)\Big)^{-1}\psi\Big(s;\ \Upsilon_{P_k,I},\ \omega_4;\ \frac{1}{2},\ 0,\ 4,\ 1,\ 1\Big)-\exp\Big(-\frac{\Upsilon_{P_k,I},\ s^2}{3}\Big)\Big(4\beta\Big(\Upsilon_{P_k,I},\ \omega_4;\ \frac{16}{3}\Big)\Big)^{-1}$$

$$\cdot\psi\Big(s;\ \Upsilon_{P_k,I},\ \omega_4;\ \frac{1}{2},\ -\frac{4}{3},\ \frac{16}{3},\ \frac{3}{5},\ 1\Big)\Bigg\}\tag{27}$$

$$\xi(s;\ \Upsilon,\ \omega;\ c_1,\ c_2)\triangleq\zeta(s;\ \Upsilon,\ \omega;\ 12,\ c_1,\ c_2)+\zeta\Big(s;\ \Upsilon,\ \omega;\ 4,\ \frac{4}{3}c_1,\ c_2\Big),$$

$$\chi(s;\ \Upsilon,\ \omega;\ c_1,\ c_2)\triangleq 1-\exp\big(-\rho(\Upsilon,\ \omega;\ c_1,\ 0)\rho(\Upsilon,\ \omega;\ c_1,\ 2c_2)s^2\big)+2\sqrt{\pi}c_2\omega s\,\exp\left((c_2\omega)^2s^2\right)$$

$$\cdot\Big(Q(\rho(\Upsilon,\ \omega;\ c_1,\ c_2)s\sqrt{2})-Q(c_2\omega s\sqrt{2})\Big),$$

$$\rho(\Upsilon,\ \omega;\ c_1,\ c_2)\triangleq c_1\Upsilon\omega^{-1}+c_2\omega,\tag{28}$$

$$\psi(s;\ \Upsilon,\ \omega;\ c_1,\ c_2,\ c_3,\ c_4,\ c_5)\triangleq -1+2\,\exp\Big(-\big(\rho(\Upsilon,\ \omega;\ c_1,\ 0)\big)^2\beta(\Upsilon,\ \omega;\ c_2)s^2\Big)$$

$$+\sqrt{\pi}c_4\omega\big(\beta(\Upsilon,\ \omega;\ c_3)\big)^{-1/2}s\,\exp\left((c_4\omega)^2\big(\beta(\Upsilon,\ \omega;\ c_3)\big)^{-1}s^2\right)$$

$$\cdot\Big(2Q(c_4\omega\big(\beta(\Upsilon,\ \omega;\ c_3)\big)^{-1/2}s\sqrt{2})-4Q(-\rho(\Upsilon,\ \omega;\ c_1,\ c_5)\big(\beta(\Upsilon,\ \omega;\ c_3)\big)^{-1/2}s\sqrt{2})$$

$$\Phi_{16}^{\mathrm{LM},1}(s|b_1=0,\ \boldsymbol{I},\ \lambda)$$

$$=\int_0^{\infty}\mathbb{E}\Big(\exp\left(sL_{\mathrm{A},16}^{\mathrm{LM},1}\right)\Big)\cdot 2\alpha\,\exp\left(-\alpha^2\right)\mathrm{d}\alpha$$

$$\simeq\sum_{p_{1,k}=0}^{1}\cdots\sum_{p_{\hat{m}-1,k}=0}^{1}\sum_{p_{\hat{m}+1,k}=0}^{1}\cdots\sum_{p_{N_B,k}=0}^{1}\prod_{m=1,\,m\neq\hat{m}}^{N_B}\left((1-\lambda)(1-p_{m,k})+\lambda p_{m,k}\right)$$

$$\cdot\frac{1}{2}\Bigg\{\frac{1}{2}\phi_1\Big(s\sqrt{\Upsilon_{P_k,I,\lambda}}\Big)\big(\phi_2(-\omega_{16}s)+\phi_2\big(-2\omega_{16}s\big)\big)+\xi(s;\ \Upsilon_{P_k,I,\lambda},\ \omega_{16};\ 16,\ 2)+\xi(s;\ \Upsilon_{P_k,I,\lambda},\ \omega_{16};\ 36,\ 2)$$

$$+\kappa\Big(s;\ \Upsilon_{P_k,I,\lambda},\ \omega_{16};\ 25,\ 1,\ \frac{8}{3},\ \frac{1}{5},\ 4,\ 15,\ \frac{20}{3}\Big)-\xi(s;\ \Upsilon_{P_k,I,\lambda},\ \omega_{16};\ 4,\ -1)-\kappa\Big(s;\ \Upsilon_{P_k,I,\lambda},\ \omega_{16};\ 36,\ 2,\ 4,\ \frac{1}{6},\ 4,\ 12,\ 0\Big)$$

$$+\xi(s;\ \Upsilon_{P_k,I,\lambda},\ \omega_{16};\ 4,\ 1)-\kappa\Big(s;\ \Upsilon_{P_k,I,\lambda},\ \omega_{16};\ 4,\ 1,\ \frac{5}{3},\ \frac{1}{2},\ 1,\ 0,\ -\frac{4}{3}\Big)-\xi(s;\ \Upsilon_{P_k,I,\lambda},\ \omega_{16};\ 9,\ 1)$$

$$+\kappa\Big(s;\ \Upsilon_{P_k,I,\lambda},\ \omega_{16};\ 4,\ -1,\ -\frac{1}{3},\ \frac{1}{2},\ 3,\ 8,\ \frac{20}{3}\Big)+\xi(s;\ \Upsilon_{P_k,I,\lambda},\ \omega_{16};\ 16,\ 1)-\kappa\Big(s;\ \Upsilon_{P_k,I,\lambda},\ \omega_{16};\ 16,\ 1,\ \frac{7}{3},\ \frac{1}{4},\ 3,\ 8,\ \frac{8}{3}\Big)$$

$$-\xi(s;\ \Upsilon_{P_k,I,\lambda},\ \omega_{16};\ 25,\ 1)+\kappa\Big(s;\ \Upsilon_{P_k,I,\lambda},\ \omega_{16};\ 9,\ 1,\ 2,\ \frac{1}{3},\ 2,\ 3,\ 0\Big)+\xi(s;\ \Upsilon_{P_k,I,\lambda},\ \omega_{16};\ 4,\ -2)$$

$$-\kappa\Big(s;\ \Upsilon_{P_k,I,\lambda},\ \omega_{16};\ 1,\ -1,\ -\frac{2}{3},\ 1,\ 2,\ 3,\ \frac{8}{3}\Big)-\kappa\Big(s;\ \Upsilon_{P_k,I,\lambda},\ \omega_{16};\ 16,\ 2,\ \frac{10}{3},\ \frac{1}{4},\ 2,\ 0,\ -\frac{16}{3}\Big)$$

$$+\kappa\Big(-s;\ \Upsilon_{P_k,I,\lambda},\ \omega_{16};\ 1,\ -1,\ -\frac{4}{3},\ -1,\ 0,\ -1,\ -\frac{4}{3}\Big)$$

$$-\kappa\Big(-s;\ \Upsilon_{P_k,I,\lambda},\ \omega_{16};\ 4,\ -2,\ -\frac{8}{3},\ -\frac{1}{2},\ 0,\ -4,\ -\frac{16}{3}\Big)\Bigg\}\tag{29}$$

IET Commun., 2016, Vol. 10, Iss. 1, pp. 24–33

$$
\begin{aligned}
\Phi_{16}^{\mathrm{LM},2}(s|b_2=0,\ \boldsymbol{I},\ \lambda) &= \int_0^{\infty} \mathbb{E}\Big(\exp\left(sL_{\mathrm{A},16}^{\mathrm{LM},2}\right)\Big)\cdot 2\alpha\,\exp\left(-\alpha^2\right)\mathrm{d}\alpha \\
&\simeq \sum_{p_{1,k}=0}^{1}\cdots\sum_{p_{\hat{m}-1,k}=0}^{1}\sum_{p_{\hat{m}+1,k}=0}^{1}\cdots\sum_{p_{N_B,k}=0}^{1}\prod_{m=1,m\neq\hat{m}}^{N_B}\left((1-\lambda)(1-p_{m,k})+\lambda p_{m,k}\right) \\
&\quad\cdot\left\{\frac{1}{2}\phi_1\Big(s\sqrt{\Upsilon_{P_k,I,\lambda}}\Big)\phi_2\left(-\omega_{16}s\right)+\xi(s;\ \Upsilon_{P_k,I,\lambda},\ \omega_{16};\ 16,\ 1)\right. \\
&\quad+\xi(s;\ \Upsilon_{P_k,I,\lambda},\ \omega_{16};\ 4,\ 1)-\kappa\Big(s;\ \Upsilon_{P_k,I,\lambda},\ \omega_{16};\ 16,\ 1,\ \frac{7}{3},\ \frac{1}{4},\ 3,\ 8,\ \frac{8}{3}\Big) \\
&\quad-\xi(s;\ \Upsilon_{P_k,I,\lambda},\ \omega_{16};\ 4,\ -1)+\kappa\Big(s;\ \Upsilon_{P_k,I,\lambda},\ \omega_{16};\ 4,\ -1,\ -\frac{1}{3},\ \frac{1}{2},\ 3,\ 8,\ \frac{20}{3}\Big) \\
&\quad\left.-\kappa\Big(s;\ \Upsilon_{P_k,I,\lambda},\ \omega_{16};\ 4,\ 1,\ \frac{5}{3},\ \frac{1}{2},\ 1,\ 0,\ -\frac{4}{3}\Big)\right\},
\end{aligned}
\tag{30}
$$

$$
\begin{aligned}
&\kappa(s;\ \Upsilon,\ \omega;\ c_1,\ c_2,\ c_3,\ c_4,\ c_5,\ c_6,\ c_7) \\
&\triangleq\begin{cases}
\zeta(s;\ \Upsilon,\ \omega;\ 12,\ c_1,\ c_2)+\exp\left(-\Upsilon s^2/3\right)\zeta\Big(s;\ \Upsilon,\ \omega;\ 4,\ \frac{4}{3}c_1,\ c_3\Big), & s\geq 0 \\
\exp\left(\Upsilon s^2\right)\chi(s;\ \Upsilon,\ \omega;\ c_4,\ c_5) & \\
+\left(12\beta(\Upsilon,\ \omega;\ c_1)\right)^{-1}\psi(s;\ \Upsilon,\ \omega;\ c_4,\ c_6,\ c_1,\ c_2,\ c_5) & \\
+\exp\left(-\Upsilon s^2/3\right)\Big(4\beta\Big(\Upsilon,\ \omega;\ \frac{4}{3}c_1\Big)\Big)^{-1}\psi\Big(s;\ \Upsilon,\ \omega;\ c_4,\ c_7,\ \frac{4}{3}c_1,\ c_3,\ c_5\Big), & s<0.
\end{cases}
\end{aligned}
\tag{31}
$$